Measurement of the environmental radiation with gamma spectroscopy techniques

Physics laboratory - 16/12/2023
Group 3
Marchesini Davide - 2121242
Lorenzo Frigato - 2109747
Aneesh Suresh Nene - 2004982

1 Abstract

Since the explosion of the first atomic bomb, one of the main public health concerns has been the presence of nuclear radiation in the public and private environment. Although the most dangerous radiation sources are coming from man activities, the vast majority of radiation in the environment has a natural origin and has always been present. In this report, to study in a proper way the environmental radiation present in some organic and inorganic samples, we will study first the properties of a HPGe and a NaI(TI) detectors, in order to obtain the best possible energy resolution for both. We will calibrate in energy the later and a characterization of their efficiency in function of the energy will be performed. A measure of the ambient background is also needed, to identify possible sources of contamination due to other radioisotopes present in the laboratory environment. We will finally measure the environmental radioactivity of the samples and, also, we will perform a Radon contamination measurement according to the U.S. Environmental Protection Agency (EPA) standard.

2 Experimental setup

A scheme of the experimental apparatus is provided in figure 1. In this experience a Hyper Pure Germanium detector (HPGe) is used due to his low resolution, that allow us to discriminate and identify correctly different gamma peaks coming from different sources decays. A Sodium Iodide detector (NaI(Tl)) is also used simultaneously with the first, as a reference for the precision measurement performed with the HPGe. Both detector are then connected to a CAEN digitizer for data acquisition (DAQ). The HPGe detector is kept at the temperature of liquid nitrogen inside of a large dewar, and can operate outside of it for a maximum of 8 hours, before the temperature becomes too high to allow proper operation of the detector. Both detectors are shielded from the outside thanks to a lead cockpit, that can be opened from the above. Nevertheless, the shielding is not complete, since some free space is left to insert the detector in the cockpit. For that reason, a background measurement is necessary, to improve the precision of the gamma spectroscopy. The latter is addressed in the following "Background analysis" section. During the measurement for the estimation of the efficiency of both detectors, there were placed source, as indicated into the figure 1, to some known distances from the center of the detectors. This distances were measured as $d_1 = (28.5 \pm 0.2)$ cm and $d_2 = (20.9 \pm 0.2)$ cm. Please refer to the "Efficiency of the detectors" section for more details.

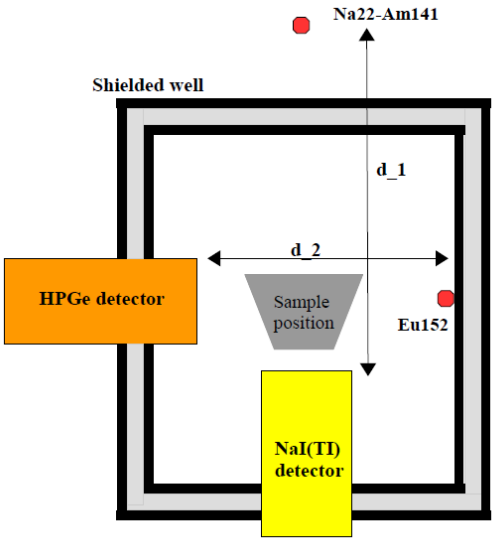

Figure 1: Experimental set-up

3 Characterization of the detectors

3.1 Optimization of the resolution

In order to get an estimate of the energy of the acquired events a trapezoidal filter is used for both detectors. The resolution obtained using this filter depends strongly on the parameters that characterize the latter, such as the value of the decay time, of rise time and of the flattop. It is therefore necessary, in order to obtain the best possible experimental resolution and to make the most of the potentialities of both detectors, to perform a scan of the possible values for the parameters of the trapezoidal filter to find the best ones, i.e. the ones that will minimize the resolution of the detector. Thus, the following method was utilized for both detectors, where the parameters were changed through the VERDI program interface.
First, we selected "by eye" a rough estimate of the decay time, in order to obtain the wanted trapezoidal form of the filter. Then, one parameter was changed at the time, leaving all the other fixed. Subsequently, a two minutes run was performed for the ^{22}Na source and a gaussian fit was performed in the 1275 keV peak in order to calculate the efficiency in function of the parameter that was changed. A scan of the efficiency in function of the possible parameter values was therefore obtained. Once the best parameter was found, the latter was fixed permanently and the procedure was iterated for the next one. In this way, minimizing the efficiency with respect to the rise time, then to the flattop and finally with respect to the decay time, we were able to obtain the best possible experimental efficiency for both detectors for the 1275 keV photon:

$$R_{NaI(Tl)} = 4,95\% \pm 0,02\% \quad R_{HPGe} = 0,194\% \pm 0,002\%$$

In figure 2 are showed the scans on the various parameter performed to minimize the resolution.

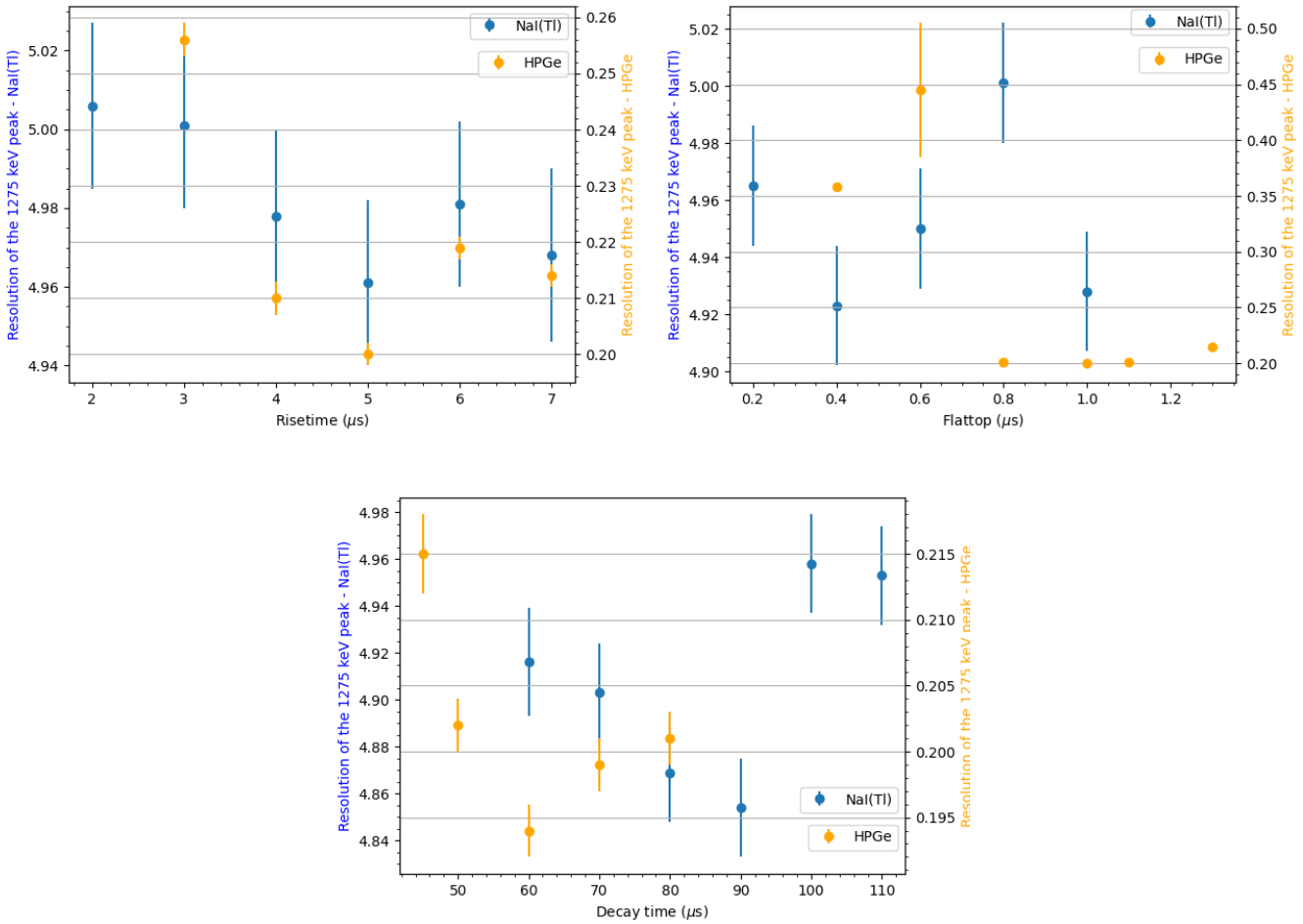

Figure 2: Resolution of the detectors for the 1275 keV photon in function of the rise time, the flattop and the decay time parameters of the trapezoidal filter

3.2 Energy calibration

To acquire meaningful data, it is also necessary to set up a proper threshold of the DAQ (to cut out the electric noise of the apparatus) and perform an energy calibration of the detectors. The threshold was set for both detectors from the VERDI interface, performing a live acquisition of the ^{241}Am spectrum as reference to make sure we did not miss low-energy events. Consequently, we can perform a calibration of the acquired spectrum, converting it from the DAQ arbitrary unit (ADC Analog to Digital Converter units) in energy (keV). A linear response of the detector is assumed

$$E_\gamma = N_{ADC} \cdot b + a \tag{1}$$

allowing us to properly calibrate our data. Therefore the following procedure was followed for both detectors. We acquired a spectrum for the ^{22}Na and one for the ^{241}Am, in order to gain accuracy in the low energy region. We then performed Gaussian fits over the peaks in order to derive the position of the peak. Then, a linear fit was executed, to find the b (angular coefficient) and a (offset) of the calibration. The experimental known values E_γ of the peaks were retrieved from the National Nuclear Data Center (NNDC) online data service [1]. We here show in figure 3 the linear calibration fits performed. The results of the Gaussian and linear fits are reported in the tables 1 and 2.

		HPGe		NaI(Tl)	
Source	Tabulated energy (keV)	Mean	σ_{Mean}	Mean	σ_{Mean}
Na 22	511	4206.89	0.04	5181.0	0.2
Na 22	1275	10494.70	0.08	12528.8	0.8
Am 241	59	490.25	0.03	665.3	0.1

Table 1: Gaussian fit results on the spectrum peaks (expressed in Analog to Digital Converter unit - ADC) for the calibrations of both detectors.

HPGe		NaI(Tl)	
b	a	b	a
(0.12156 ± 0.00004) keV/ADC	(-0.6 ± 0.1) keV	(0.101 ± 0.001) keV/ADC	(-8 ± 2) keV

Table 2: Results of the linear fits for the calibration of both detectors.

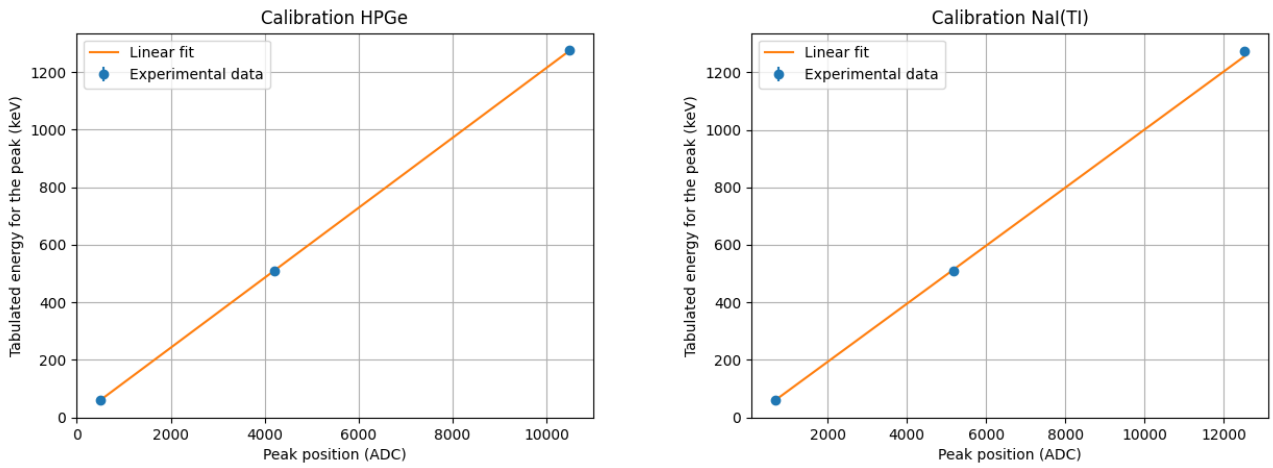

Figure 3: Calibration fit for the HPGe detector (right) and for the NaI(TI) detector (left).

3.3 Background analysis

We performed two background measurement, one with the cockpit open - to identify the major sources of contamination - and one with the closed cockpit, that will be used to correct the experimental spectrum

acquired. To identify the peaks and the relative radioisotopes present in the environment we used as a reference the NNDC database [1] and the Decay Data Evaluation Project (DDEP) table of radionuclides [2]. In figure 4 are shown the background measurements taken for the HPGe detector.

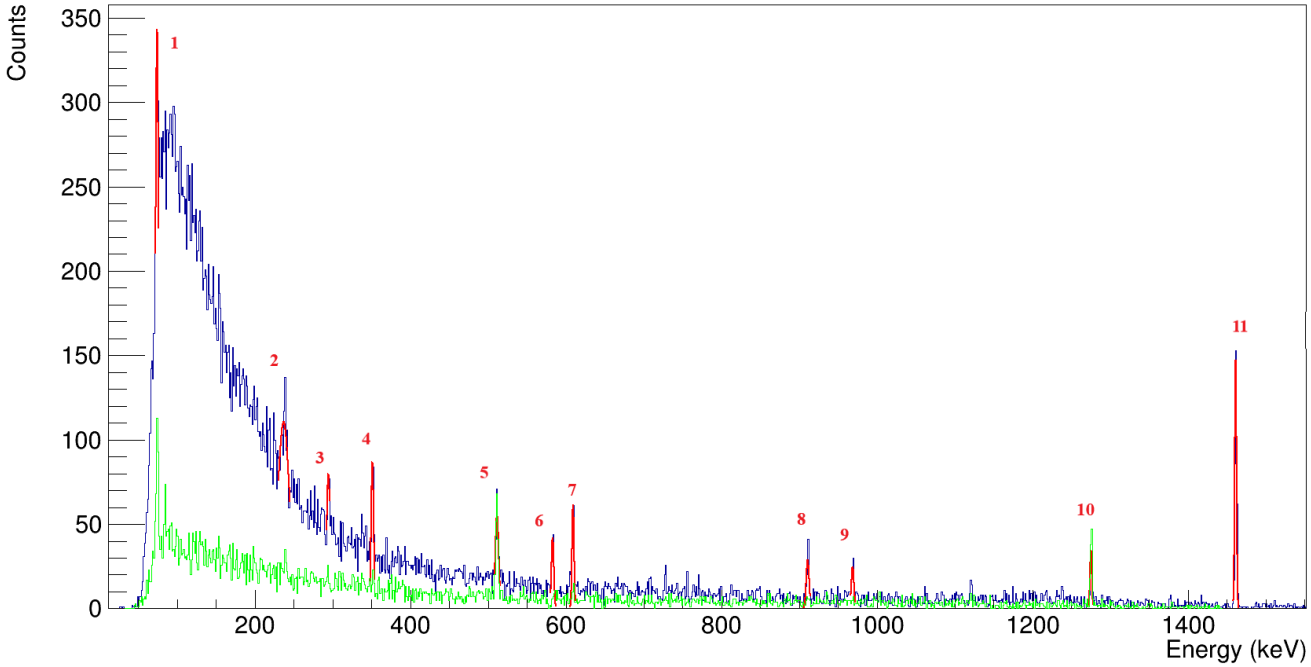

Figure 4: Background measurement in blue with the cockpit open while in green with the cockpit closed. In red there are the peaks considered and the relative gaussian fits.

It is possible to identify clearly 11 peaks, which are reported in the table 3. A prominent peak is coming from the ^{40}K, which is present in the concrete walls of the laboratory and therefore surrounds the experimental set-up. It is also possible to identify the two peaks due to the decay of the ^{22}Na, where the 511 keV peak is probably also due to every source of positron (i.e. every nuclei that has a β^+ decay) present in the laboratory. We were able to identify the peaks belonging to ^{214}Pb and ^{214}Bi radioisotopes, which are probably coming from the ^{222}Ra chain decay. Furthermore, we also identify the peaks related to the ^{212}Pb, ^{208}Tl and the ^{228}Ac radioisotopes, that are instead probably coming from the decay chain of the ^{232}Th. It is also present a non negligible initial peak of $74.2keV$, that is compatible with the X rays emitted in the decay of both ^{214}Pb and ^{212}Pb. From the figure 4 it is also possible to see that once the cockpit was closed, all the sources of contamination and their peaks vanish, except for the two peaks of the ^{22}Na, that present a similar intensity with both the cockpit open and closed.

Peak	**Peak Energy**	**Identified Element**	**Tabulated Energy**
1	(74.2 ± 0.2) keV	$Xrays$	74.81 keV
2	(238.2 ± 0.5) keV	^{212}Pb	238.63 keV
3	(294.1 ± 0.5) keV	^{214}Pb	295.22 keV
4	(351.2 ± 0.1) keV	^{214}Pb	351.93 keV
5	(510.4 ± 0.2) keV	^{22}Na	511.00 keV
6	(583.4 ± 0.2) keV	^{208}Tl	583.19 keV
7	(608.9 ± 0.1) keV	^{214}Bi	609.32 keV
8	(910.2 ± 0.2) keV	^{228}Ac	911.21 keV
9	(968.4 ± 0.2) keV	^{228}Ac	968.97 keV
10	(1274.8 ± 0.1) keV	^{22}Na	1275.58 keV
11	(1460.75 ± 0.06) keV	^{40}K	1460.82 keV

Table 3: Identified peaks and relative radioisotpes for the laboratory background.

3.4 Efficiency of the detector: intrinsic and relative efficiency

To calculate the efficiency of the NaI detector we used the sources ^{22}Na and ^{241}Am, positioned as show in the figure 1, at a distance d_1 from the center of the detector. After collecting a spectrum (with the opened cockpit), to calculate the number of events under each photopeak we performed fits over the peaks with a function $f(E) = gaussian + linear$, to compensate for the Compton continuum. From this fits we can calculate number of events under each peak as the integral of the fitted gaussian, that is given by $N = \sqrt{2\pi}A\sigma$, properly divide for the bin width,where A and σ are the gaussian fitted parameter. The total absolute efficiency is given by the product of the intrinsic efficiency ϵ_{intr} and the geometric efficiency ϵ_{geo}, which takes into account the portion of solid angle under the detector, that is $\Sigma/4\pi r^2$ (where r the distance from the source to the detector and Σ the area of the detector). We therefore obtain

$$\epsilon_{tot}(E_\gamma) = \frac{\#of\ particles\ revealed}{\#of\ particles\ emitted} = \epsilon_{intr}(E_\gamma) \cdot \epsilon_{geo} = \frac{N_\gamma}{T \cdot A \cdot \Gamma} \tag{2}$$

$$\epsilon_{intr}(E_\gamma) = \frac{\#of\ particles\ revealed}{\#of\ particles\ in\ the\ detector} = \frac{N_\gamma}{T \cdot A \cdot \Gamma} \cdot \frac{4\pi r^2}{\Sigma} \tag{3}$$

with A the measured nominal activity of the sources - which is 392.2 kBq for the ^{22}Na and 420.32 kBq for the ^{241}Am, T the duration of the measure and Γ is the fraction of events that produces the gamma transition of interest (i.e. the branching ratio of the process; $0 \leq \Gamma \leq 1$), which multiplied together give the total number of photon emitted by the source. Nevertheless, the intrinsic efficiency is a function of the energy of the photon emitted, $\epsilon_{intr}(E_\gamma)$, therefore is only possible to calculate it for the given energy of the peaks, and not give a general value. The values obtained for the NaI detector are provided in the table 4.

Energy [keV]	ϵ_{intr}^{NaI}
59.30 ± 0.06	$(58.9 \pm 1.7)\%$
513.50 ± 0.13	$(11.23 \pm 0.14)\%$
1252.60 ± 0.11	$(2.955 \pm 0.019)\%$

Table 4: Efficiency for the peaks analysed for the NaI detector for the geometry defined in 1.

For the Germanium detector, instead, we used a Europium 152 source with a nominal activity of 74.7 kBq, positioned as shown in figure 1 at a distance d_2 from the center of the detector. Since the ^{152}Eu source presents a lot of peaks, is possible to improve the efficiency curve in function of the energy of the incoming photon. The spectrum of the source is reported in the figure 5. In particular, in this case, we calculate also the relative efficiency for each photon, in which the total number of counts under each photo-peak are normalized assuming that the 1408 keV photon has yielded 100%. In an analogy as what we did for the NaI detector, we've performed the fits over the peaks, determining the counts under each peak. The fits where executed changing the bin size and the range of interest so to minimize the error on the counting numbers. Therefore we can calculated the relative efficiency as

$$\epsilon_{rel} = \frac{N(counted)}{N(tabulated)} \cdot \frac{100}{N_{1408}(counted)}$$

where the values $N(tabulated)$ are the tabulated values for the intensity of each peak assuming that the 1408 keV photon has yielded 100%. The absolute intrinsic efficiency was instead calculated as before with the use of equation 3. In order to have an analytic expression for the $\epsilon_{intr}^{HPGe}(E_\gamma)$ function, a fit on the experimental value obtained was considered. In particular, we chose to fit the data with an exponential function. Therefore, for the relative efficiency we obtain the fitting function as $y = a_{rel} \cdot exp[b_{rel} \cdot x] + c_{rel}$, obtaining the parameter values and their errors as

$$a_{rel} = (9.03 \pm 0.09) \quad b_{rel} = (-3.35 \pm 0.04) \cdot 10^{-3} \frac{1}{keV} \quad c_{rel} = (0.957 \pm 0.011) \tag{4}$$

For the absolute intrinsic efficiency we performed the same exponential fit as for the relative efficiency, with the function $y = a_{abs} \cdot exp[b_{abs} \cdot x] + c_{abs}$. We obtained the parameters values

$$a_{abs} = (103.4 \pm 1.0) \quad b_{abs} = (-3.31 \pm 0.04) \cdot 10^{-3} \frac{1}{keV} \quad c_{abs} = (10.50 \pm 0.13) \tag{5}$$

The experimental data for the efficiencies calculated for the geometry defined in the figure 1 and their fitted function are showed in the figure 6.

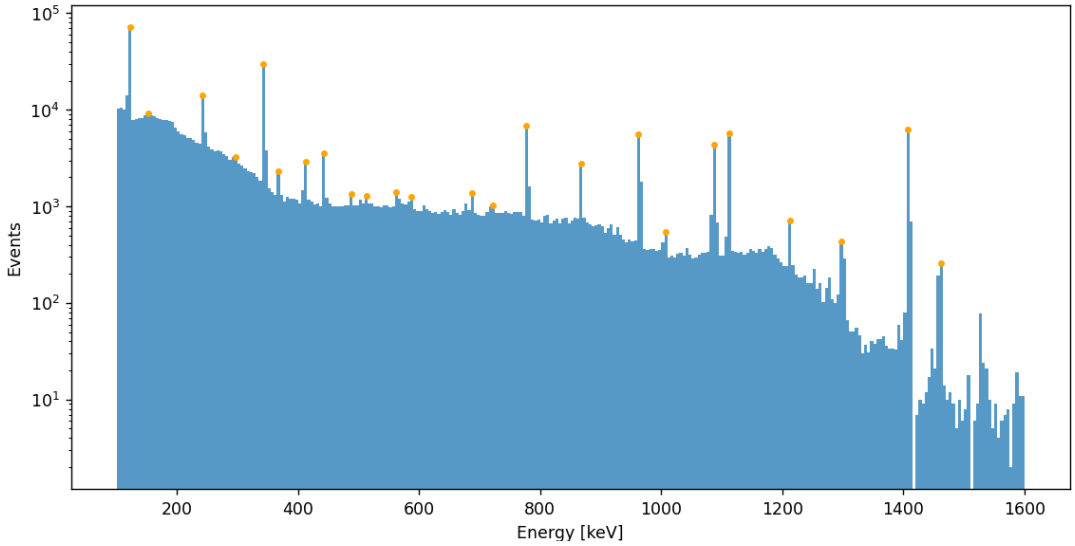

Figure 5: Spectrum of the ^{152}Eu source for an acquisition time of 20 minutes. In yellow are highlighted the Europium gamma transition considered.

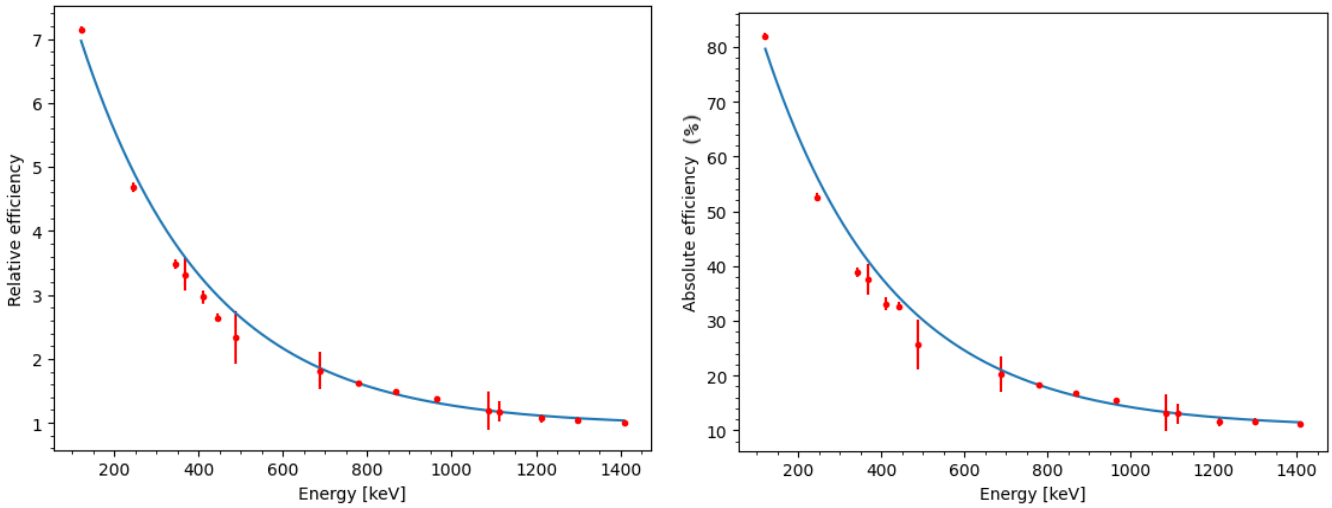

Figure 6: Relative efficiency on the left and absolute on the right as a function of the energy with the relative fitted exponential functions.

4 Samples activity analysis

We were interested in measuring three samples, one organic and two inorganic:

- (273.0 ± 0.1) g of pellets ash
- (1157.3 ± 0.1) g of zirconium oxide
- (30.2 ± 0.1) g of autunite

We acquired the 3 spectrum (figure 7) with the HPGe scintillator. In this way, following the same procedure as before, we can calculate the number of events under each photo peak. To find the activity in Bq/g of the samples we need first to correct the number of counted events to find the number of emitted particles by the source, i.e. the number of decay in the observation time. From equation 2-3

$$N_{emitted} = \frac{N_{exp}}{\epsilon_{intr}^{HPGe}(E_\gamma)} \frac{4\pi d^2}{\Sigma} \tag{6}$$

where $\epsilon_{intr}^{HPGe}(E_\gamma)$ is given by the exponential function estimated in the previous section calculated in the energy of the photpeak, E_γ, d is the distance of the source from the detector and N_{exp} is the experimental number of counts for each peak, obtained trough gaussian plus linear fit of the relative peak. The distance d

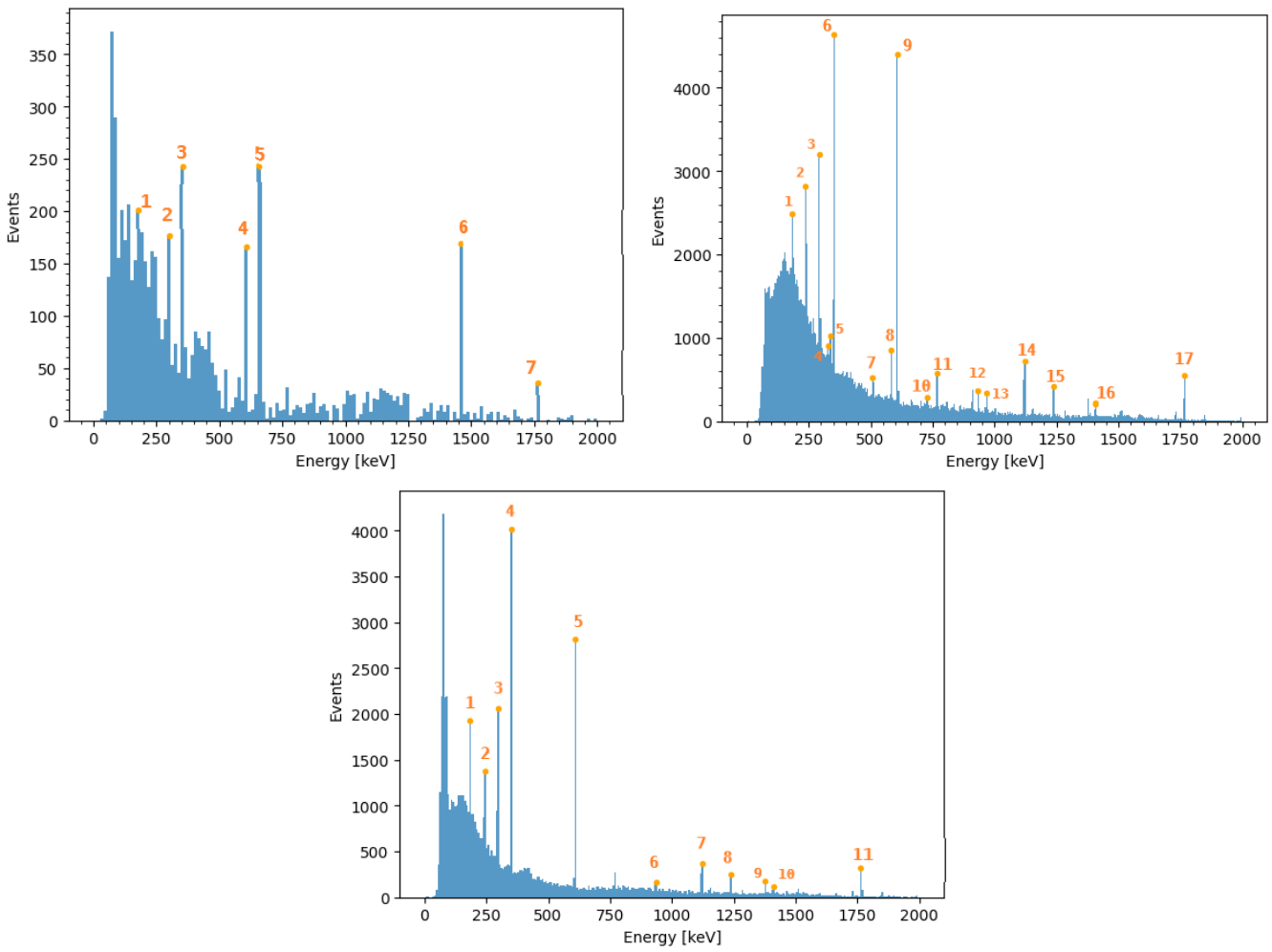

Figure 7: Spectrum of the sources collected with the relative peaks considered in the analysis that was possible to identify, marked in yellow. Starting from the top left, spectrum of pellets, zirconium and autunite

can be estimated considering the source as point-like and positioned on the center of the detector and so the solid angle correction factor is $(4\pi d^2)/\Sigma \approx 114.4$. This is a very drastic approximation, since the samples are not small enough compared to the detector to be consider as point like, but nevertheless necessary to make progress with the calculations. The activity per gram of the peaks will finally be estimated as

$$A_\gamma = \frac{N_{emitted}}{\Delta T \cdot m} \tag{7}$$

where ΔT is the observation time and m is the mass of the source. The total activity A of the source will be simply the total sum of the activity of all the peaks of the source. Following this procedure we found the following peaks, presented in the tables 5-6-7, which are associated to a given radio isotope presents in the sample.

Peak no.	Energy [keV]	Activity [Bq/g]	Identified element	Tabulated energy [keV]
1	185.3 ± 0.4	0.022 ± 0.007	^{235}U	185.72
2	295.2 ± 0.1	0.059 ± 0.01	^{214}Pb	295.22
3	351.49 ± 0.09	0.109 ± 0.009	^{214}Pb	351.93
4	609.2 ± 0.3	0.13 ± 0.02	^{214}Bi	609.32
5	661.8 ± 0.2	0.232 ± 0.02	^{137}Cs	661.66
6	1461.67 ± 0.06	0.322 ± 0.007	^{40}K	1460.822
7	1765.3 ± 0.2	0.067 ± 0.006	^{214}Bi	1764.49
	Total Activity	1.0 ± 0.1		

Table 5: Analysis on the Pellet ash sample.

We can notice that the major part of the peaks identified arose from the ^{238}U chain and the ^{232}Th. This is expected, since they are one of the most prominent sources of natural radioactivity and some of the relative

Peak no.	Energy [keV]	Activity [Bq/g]	Identified element	Tabulated energy [keV]
1	185.50 ± 0.05	0.074 ± 0.007	^{235}U	185.72
2	239.6 ± 0.2	0.25 ± 0.03	^{212}Pb	238.63
3	269.7 ± 0.3	0.05 ± 0.01	^{228}Ac	270.20
4	294.7 ± 0.01	0.281 ± 0.006	^{214}Pb	295.22
5	338.0 ± 0.1	0.032 ± 0.006	^{228}Ac	338.30
6	351.61 ± 0.01	0.06 ± 0.01	^{214}Pb	351.93
7	510.45 ± 0.07	0.064 ± 0.006	^{22}Na	511.00
8	582.98 ± 0.05	0.129 ± 0.009	^{208}Tl	583.19
9	609.183 ± 0.007	0.98 ± 0.01	^{214}Bi	609.32
10	727.2 ± 0.3	0.030 ± 0.008	^{212}Bi	727.33
11	768.42 ± 0.05	0.12 ± 0.01	^{98}Zr	768.40
12	934.39 ± 0.08	0.089 ± 0.008	^{92}Zr	934.47
13	968.9 ± 0.1	0.09 ± 0.01	^{94}Zr	969.00
14	1120.70 ± 0.01	0.44 ± 0.03	^{214}Bi	1120.29
15	1238.6 ± 0.1	0.16 ± 0.01	^{214}Bi	1238.11
16	1408.5 ± 0.5	0.07 ± 0.03	^{152}Eu	1408.00
17	1765.50 ± 0.03	0.378 ± 0.005	^{214}Bi	1764.49
	Total Activity	4.1 ± 0.3		

Table 6: Analysis on the Zirconium Oxide sample.

Peak no.	Energy [keV]	Activity [Bq/g]	Identified element	Tabulated energy [keV]
1	185.54 ± 0.02	3.1 ± 0.1	^{235}U	185.72
2	241.53 ± 0.05	3.8 ± 0.1	^{214}Pb	241.98
3	294.77 ± 0.02	9.3 ± 0.2	^{214}Pb	295.22
4	351.557 ± 0.006	18.09 ± 0.09	^{214}Pb	351.93
5	609.204 ± 0.005	24.0 ± 0.2	^{214}Bi	609.32
6	934.23 ± 0.08	2.1 ± 0.2	^{214}Bi	934.06
7	1120.77 ± 0.04	8.6 ± 0.3	^{214}Bi	1120.29
8	1238.80 ± 0.08	3.5 ± 0.2	^{214}Bi	1238.11
9	1378.38 ± 0.07	2.2 ± 0.3	^{214}Bi	1377.67
10	1408.9 ± 0.2	1.2 ± 0.3	^{152}Eu	1408.00
11	1765.7 ± 0.2	7.1 ± 0.7	^{214}Bi	1764.49
	Total Activity	87 ± 4		

Table 7: Analysis on the Autunite sample.

radioisotopes were also already found in the background measure. However, we would like to emphasize the presence of some particularly interesting isotopes detected in our samples. For instance, an interesting one is found in the pellet ash sample: we found a peak for ^{137}Cs which comes from human activities, such as fission in nuclear reactors or in nuclear explosion test in the atmosphere. A part of it could also come from remnant of Chernobyl, or other nuclear disasters. We also observe for the pellet ash a prominent ^{40}K peak. This was expected since plants absorb K from the soil which might also contain isotope of K. For what concerns the autinite mineral, it's known that its molecular formula is $Ca(UO_2)_2(PO_4)_2 \cdot 10-12H_2O$. This mineral therefore contains uranium and in fact we can observe a very high activity of the sample, with the presence of elements coming from the decay chain of both ^{235}U and ^{238}U, the two most commons isotopes of U. For the compound zirconium oxide (ZrO_2), instead, we can observe traces of various isotopes of Zr, as one could expect. A 511 keV peak is also present: this could derive both from the decay of ^{22}Na and from any other nucleus that decays β^+ and produces a positron, thus giving rise to an annihilation e^+e^-.

Furthemore, we could also perform the very same calculation for the NaI detector, trying to estimate the activity of the samples with it. Plotting an example in figure 8 we observed that in this case the peaks overlap with each other. Thus, performing any sort of gaussian fit would not determine the correct number of events under a certain peak because it will count also events on the neighboring ones. A complete de-convolution of the spectrum would be necessary.

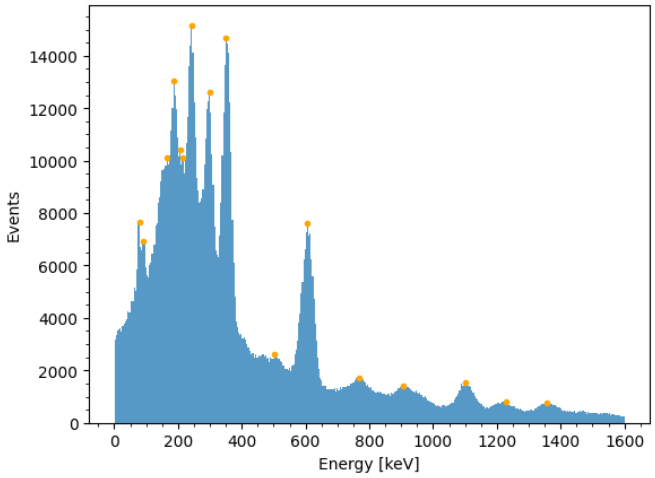

Figure 8: Example of spectrum with the NaI detector, Zirconium oxide

5 Radon study

To determine the activity of the radon presence in our laboratory (situated in Padua, Veneto) we performed a radon measure according to the EPA standard. We used a canister of activated charcoal that was weighted and left open for 48 hours in a basement room of the laboratory complex. After the appropriate amount of time, the radon has been absorbed by the canister, trapped inside the atmosphere humidity drops, and we can recore the canister. The difference of weight before and after the exposition, i.e. the water gain, was of (4.7 ± 0.1) g. We can therefore fix the average humidity to 80% according to the EPA standard. This is expected, since during the measurement period it has always been raining. So, we can calculate the calibration factor CF, which indicates how many liters per air are filtered per minute by the canister, as

$$CF = \frac{CF(2)AF(T)}{AF(2)} = CF(2) \approx 0.11 \quad \frac{L}{min}$$

with the AF coefficients that are time depend factors. The latter relate the CF coefficient for 48 hours exposure time to the CF relative to the actual exposure time, T. Since the time of exposure was already of 48 hours their ratio is 1, and the CF coefficient can be estimated as $CF(2)$, that can be retrieved from the EPA's tabulated data. Then, we can calculate the decay factor DF, which correct for the fact that part of the captured radon can decay before the measurement so it is not observed in the spectrum, as

$$DF = exp(-\frac{0.693 \cdot t}{5501}) \approx 0.828$$

where $T_{1/2} = 5501$ min is the half life of the radon 222 and t is the time from half the exposure time of the canister to the actual measurement time. This time can be estimated as $t \approx 25 \quad hours$, and therefore the appropriate coefficient can be calculated. Finally the radon activity per liter of air is calculated, according to the EPA standard, as

$$RN = \frac{N}{DF \cdot E \cdot CF \cdot T_s} \tag{8}$$

where E is the net number of counts per week per pico-Curie for the standard Radium 226 calibration source, which has a tabulated activity of 0.37 kBq, N is the net number of counts measured in the exposed canister per week and T is the exposure time, measured in minutes. To estimate N and E we collected three spectrum: one for the canister that was exposed in the basement, that will give us N; one for a standard reference radon source with known activity and the same geometry of the canister, that will give us E; and one for an empty canister, that it is used as background for the other measurements. Each spectrum was taken during a 30 minutes long acquisition, except for the reference source that, due to lack of time, was only 5 minutes long, but however sufficient to have enough statistics. To estimate the total number of counts emitted by the sources we can proceed as in the previous section, using equation 6. The acquired spectrum are presented in figure 9, with the considered peaks, while in the tables 8 are reported the identified radio isotopes. Unfortunately it wasn't possible to identify all the peaks.
It is possible to see that the 185 keV (highlighted in bold in table 8) peak is missing in the canister spectrum, that is instead present in the radium one. This is because the latter is the result of the α decay of the ^{226}Ra

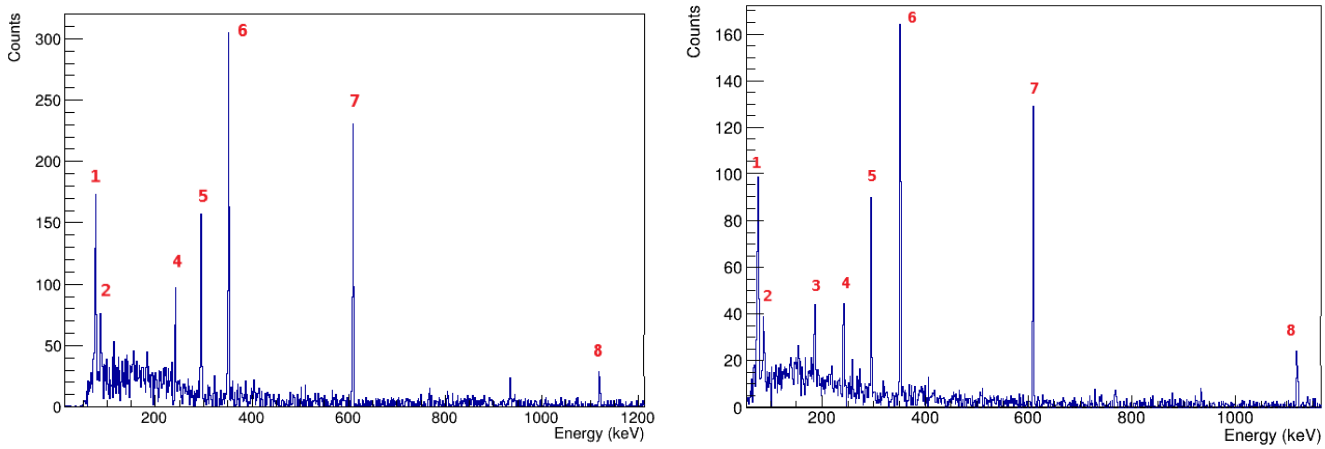

Figure 9: On the left is presented the spectrum of the canister we left in the basement for 2 days and the relative peaks for a 30 minutes run, on the right the spectrum and relative peaks of the standard reference Radium source for a 5 minutes run, both with the background subtracted.

Peak no.	Energy [keV]	Identified element	Tabulated energy [keV]
1	75.5 ± 0.1		
2	86.9 ± 0.2		
3	**185.55 ± 0.17**	**^{226}Ra**	**186.211**
4	241.6 ± 0.2	^{214}Pb	242.00
5	293.3 ± 0.6		
6	351.27 ± 0.06	^{214}Pb	351.93
7	609.00 ± 0.02	^{214}Bi	609.32
8	1120.2 ± 0.1	^{214}Bi	1120.30

Table 8: Photo peaks considered for the calculation of E and N.

into the ^{222}Rd, therefore it's not visible in the canister spectrum since we collect only the radon. An additional spectrum was also taken to test the EPA procedure, namely, we took a spectrum only of the canister's lid (a sponge). In this way, we wanted to test whether the moisture droplets actually remained trapped only inside the canister or whether the sponge also contributed to the collection of radon. Since it is not possible to distinguish the spectrum of the background with that of the sponge, it is evident that all radon has been absorbed by the canister, as indicated in the EPA's procedure. It is finally possible to estimate the radon activity per liter as

$$RN = (0.49 \pm 0.09) \quad \frac{Bq}{L} = (4.9 \pm 0.9) \cdot 10^3 \quad \frac{Bq}{m^3}$$

This value is an order of magnitude higher than the average values found in Veneto, of about $60 Bq/m^3$, according to ARPAV Veneto. A possible explanation could be given by the fact that the closet where the canister was placed is a small and always closed environment, which is opened only to put and remove the canister. Therefore, radon would accumulate more easily in the laboratory than in an open environment such as the physics laboratory. However, possible errors in the calculation of this activity are not excluded, even if we have not been able to find them, having repeated the procedure several times with similar results. On the other hand we can rest assured: if such high Radon concentrations were present in the laboratory frequented by the students they would surely have been noticed in the peaks taken during the background measurement. In any case the limit value imposed by Italian law in a workplace is $500 Bq/m3$. This, combined with the fact that the laboratory, as already mentioned, is an open and continuously ventilated environment will ensure that there are no dangers to our health.

6 Conclusion

In conclusion, we studied the behavior of the detectors by changing some key parameters, managing to obtain good experimental resolutions for both, which allowed us to easily identify the peaks in the continuation of

the experience. A background analysis allowed us to identify the sources of natural radioactivity present in the laboratory, allowing us to take them into account in the analysis of samples, obtaining more accurate results. With the HPGe detector we studied the selected samples analyzing the composition and the presence of radioactive elements, especially evaluating the activity over the weight. Lastly, we studied the Radon contamination in the laboratory building. We performed our calculations using the EPA standard but getting results not compatible with the expected value of an indoor measurement, even though under the limit imposed by Italian legislation.

Bibliography

[1] C.L. Dunford and T.W. Burrows. *Online Nuclear Data Service*. Report **IAEA-NDS-150**, International Atomic Energy Agency, Vienna, Austria.

[2] Laboratoire National Henri Becquerel. *Mono. BIPM-5 – Table of Radionuclides*. **Vol.8**, 2016.